Supporting information

Plasma-driven CO_2 Hydrogenation to CH_3OH over $Fe_2O_3/\gamma\text{-}Al_2O_3$ Catalyst

Shengyan Meng [a], Liang Wu [b], Miao Liu [a], Zhaolun Cui [c], Qian Chen [a], Shangkun Li [a,d], Jiahui Yan [a], Li Wang [e], Xinkui Wang [a], Ji Qian [a], Hongchen Guo [a], Jinhai Niu [b]*, Annemie Bogaerts [d] and Yanhui Yi [a]*

[a] State Key Laboratory of Fine Chemicals, School of Chemical Engineering, Dalian University of Technology, Dalian 116024, P.R. China.

[b] Liaoning Key Lab of Optoelectronic Films and Materials, School of Physics and Materials Engineering, Dalian Nationalities University, Dalian, 116600 People's Republic of China

[c] School of Electric Power Engineering, South China University of Technology, Guangzhou 510630, China.

[d] Research group PLASMANT, Department of Chemistry, University of Antwerp, Universiteitsplein 1, BE-2610 Wilrijk-Antwerp, Belgium.

[e] College of Environmental Sciences and Engineering, Dalian Maritime University, Dalian 116026, Liaoning, P. R. China.

* Corresponding author: Jinhai Niu, Yanhui Yi

E-mail address: niujh@dlnu.edu.cn, yiyanhui@dlut.edu.cn

Table of Contents

1. Schematic diagram of experimental setup and catalytic tests
2. Measurement of reaction temperature
3. Chromatography and 1H NMR results
4. Carbon balance calculation
5. Influence of the active metal and support on the CH_3OH selectivity and CO_2 conversion
6. Reaction results at different plasma catalysis conditions
7. Reaction temperature at different residence time
8. Plasma catalysis, thermal catalysis and electrocatalysis for CO_2 to CH_3OH
9. Reaction performance with different packing
10. The average particle size and dispersion
11. EDX mapping results
12. N_2 physisorption data for the spent catalysts
13. XPS results of CuO/γ-Al_2O_3 catalysts
14. XRD results of spent catalysts
15. Mössbauer parameters of fresh and spent 5 wt.% Fe_2O_3/γ-Al_2O_3 catalysts
16. TPR results of Fe_2O_3/γ-Al_2O_3 catalysts
17. XPS results of spent catalysts
18. HRTEM results of 5 wt.% Fe_2O_3/γ-Al_2O_3 spent catalyst
19. The reaction performance and H_2-TPR profiles of reduced catalyst
20. UV-Vis spectrum of γ-Al_2O_3 and Fe_2O_3/γ-Al_2O_3
21. In situ DRIFTS reaction cell
22. In situ DRIFTS spectra of the linearly adsorbed CO_{ad}
23. Possible E-R reactions in plasma-catalytic CO_2 hydrogenation to CH_3OH
24. References

1. Schematic diagram of experimental setup and catalytic tests

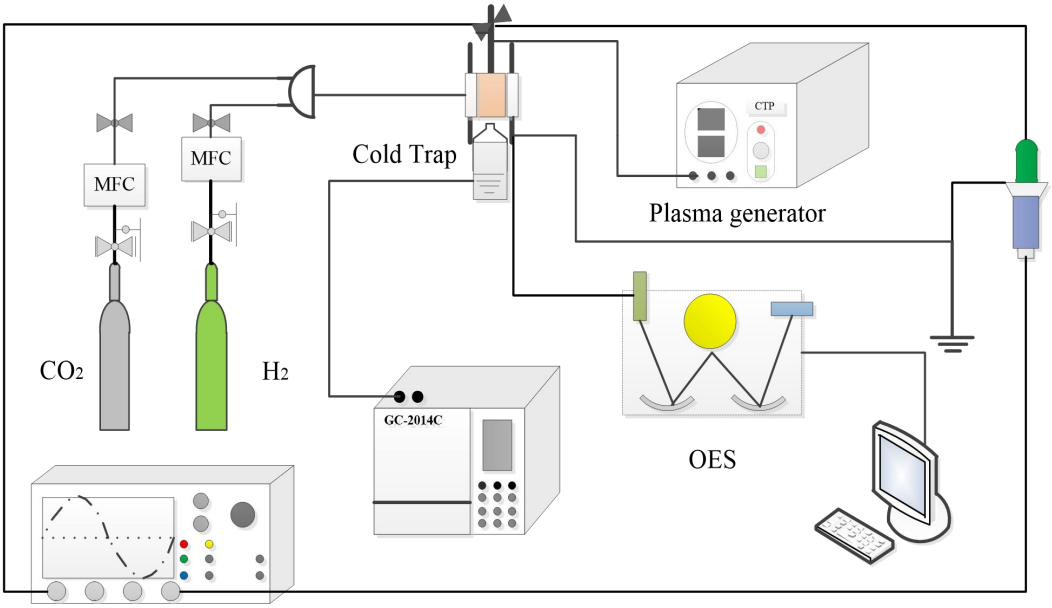

Figure S1. Schematic diagram of experimental setup

2. Measurement of reaction temperature

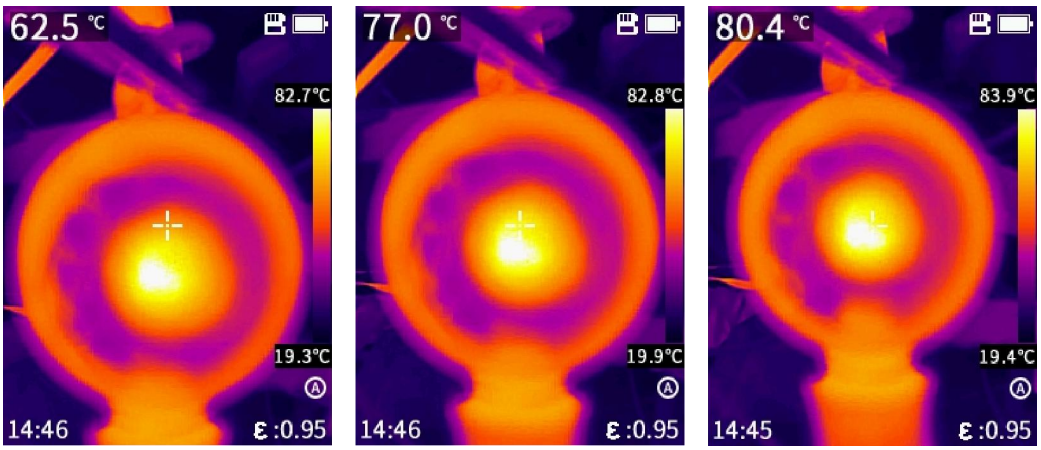

Figure S2. Temperature distribution of the DBD reactor during operation obtained by an infrared camera.

3. Chromatography and 1H NMR results

The chromatography results showed that CH_3OH concentration was 487 mg/ml. In 1H NMR, only a chemical shift at 3.33 ppm has been detected (4.79 is caused by standard D_2O solvent), and it is assigned to CH_3OH.

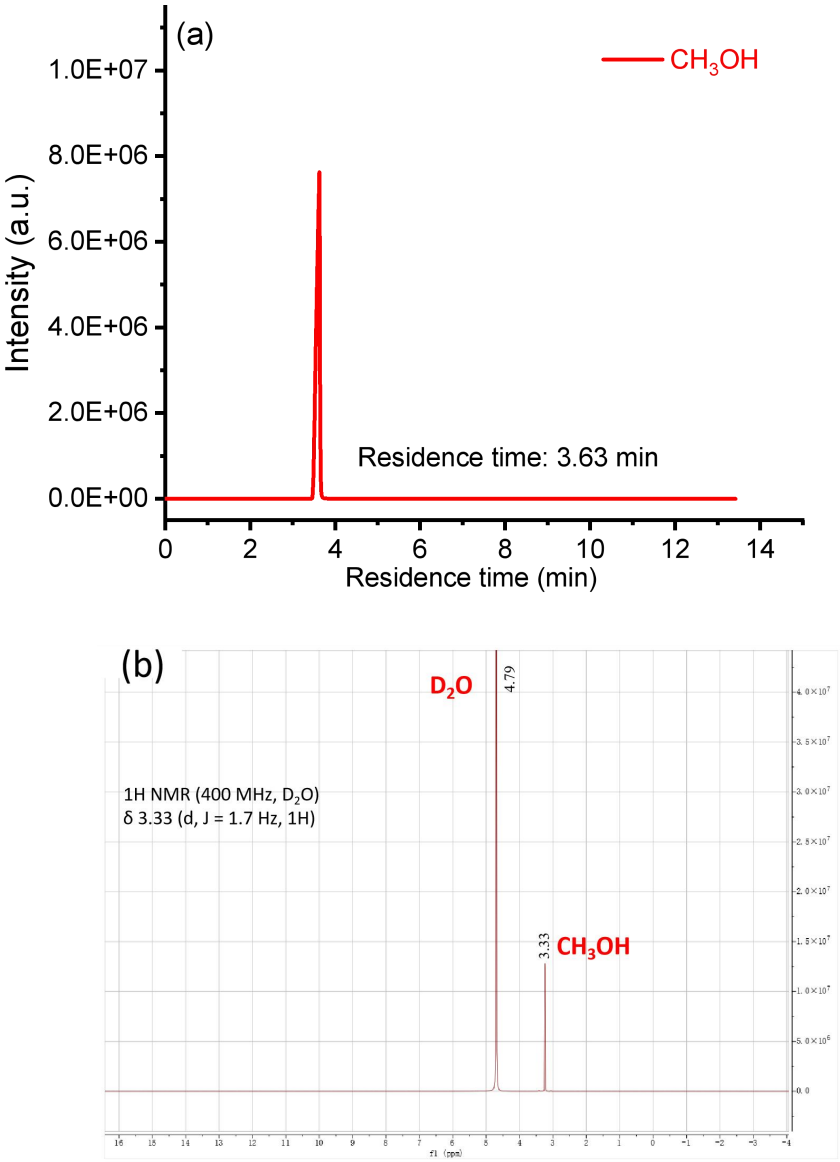

Figure S3. (a) Chromatography and (b) 1H NMR results of the liquid products.

4. Carbon balance calculation

Taking the average value of three times of plasma-catalytic CO_2 hydrogenation experiments as an example (3h reaction time), the amount of converted CO_2 was 0.01706 mol (18*60*3*0.118/22.4*1000). The chromatograph results show that the total amount of generated CO and CH_4 was 0.0073 mol. The volume of collected liquid product was about 0.5 ml (**Figure S4a**), and the concentration of CH_3OH in the liquid was 487 mg/ml (obtained by GC). That is, $S_{CO} + S_{CH4} + S_{CH3OH} = 87.4$ %, which is indeed lower than 100 %. This may be caused by some liquid residue on the catalysts, cotton and collector walls (**Figure S4c**), resulting in a smaller volume of collected liquid than the real volume of liquid products. Also, there was negligible carbon deposition (coking). If the fraction of lost liquid product is reduced, then the carbon balance may be closer to 100 %. Therefore, we have calculated the carbon balance for the 20 h continuous experiments. In this case, the amount of converted CO_2 was 0.1157 mol (18*60*20*0.12/22.4*1000), and the total amount of CO and CH_4 produced was 0.0472 mol. We collected approximately 4.2 ml liquid product with a CH_3OH concentration of 495 mg/ml (**Figure S4b**). That is, $S_{CO} + S_{CH4} + S_{CH3OH} = 96.9$ %, and thus the carbon balance in this plasma-catalytic CO_2 hydrogenation 20 h experiment is close to 100 %. The standard curves of gas (CO_2 and CO) and liquid product (CH_3OH) are shown in **Figure S4d**, with correlation coefficients (R^2) exceeding 99.8 %.

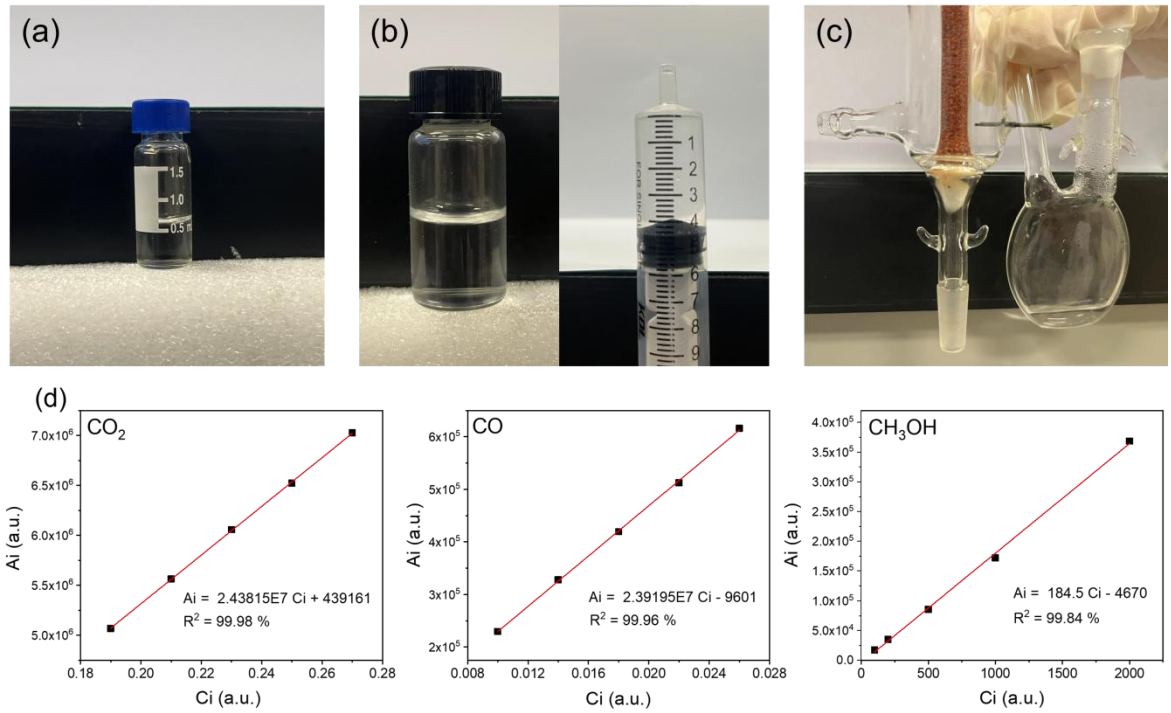

Figure S4. (a-c): The volume of collected liquid product; (d): The standard curves of CO_2, CO and CH_3OH.

5. Influence of the active metal and support on the CH_3OH selectivity and CO_2 conversion

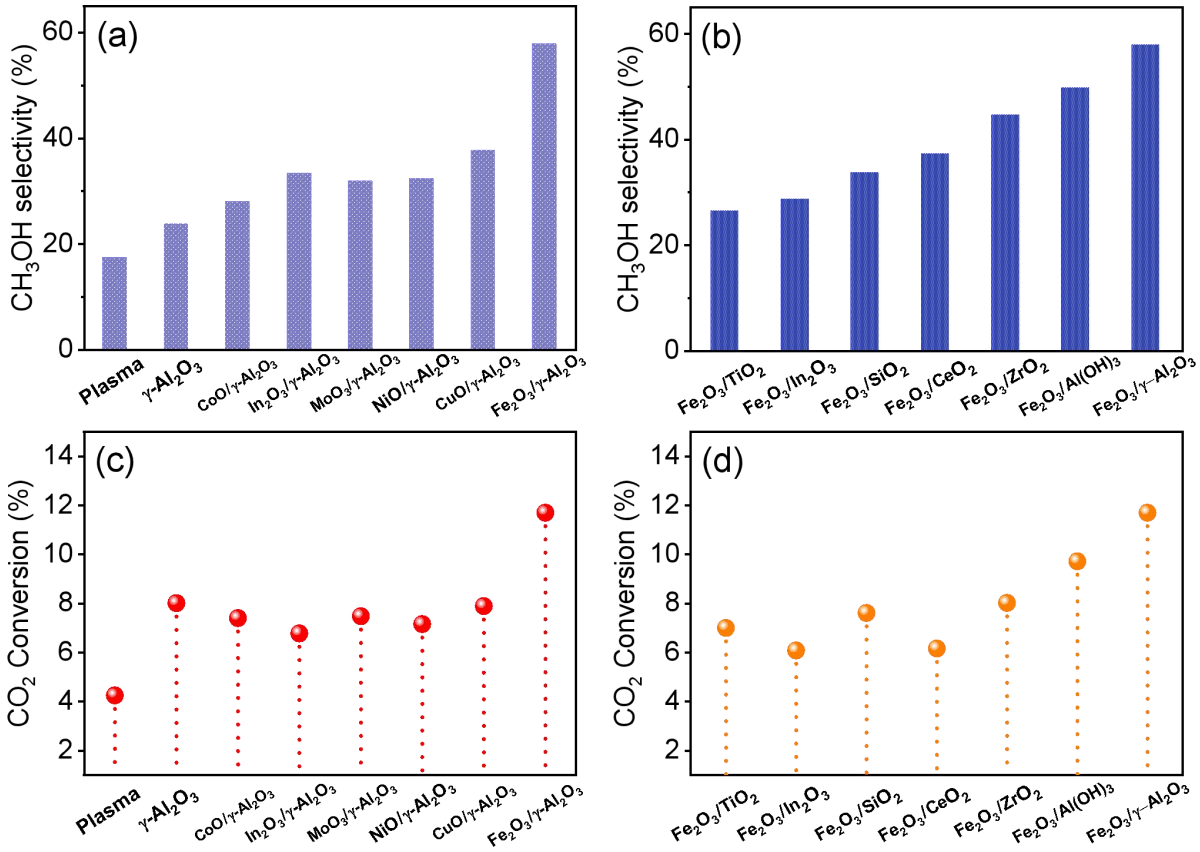

Figure S5. Performance of plasma-catalytic CO_2 hydrogenation to CH_3OH. (a) and (c): Influence of the active metal on the CH_3OH selectivity and CO_2 conversion using γ-Al_2O_3 as support; (b) and (d): Influence of the support on the CH_3OH selectivity and CO_2 conversion using Fe as active metal. (discharge power 18 W, discharge frequency 9 kHz, $CO_2/H_2 = 1/3$, residence time 3.1 s, 60 °C circulating water, 1 atm pressure);

6. Reaction results at different plasma catalysis conditions

Table S1. Reaction results at different plasma catalysis conditions.

Residence time (s)	CO_2 conversion (%)	CH_3OH selectivity (%)	CH_3OH yield (%)
7	18.8	13.4	2.52
4.7	15.1	17.9	2.70
3.9	14.4	25.8	3.72
3.1	**12.5**	**37.9**	**4.74**
2	5.3	21.0	1.11
CO_2/H_2 ratio	CO_2 conversion (%)	CH_3OH selectivity (%)	CH_3OH yield (%)
1:1	9.5	36.9	3.51
1:2	11.5	35.0	4.03
1:3	**12.5**	**37.9**	**4.74**
Discharge power (W)	CO_2 conversion (%)	CH_3OH selectivity (%)	CH_3OH yield (%)
18	**11.7**	**57.9**	**6.77**
25	12.5	37.9	4.74
30	13.9	30.3	4.21
35	14.4	21.4	3.08
Cooling temperature (°C)	CO_2 conversion (%)	CH_3OH selectivity (%)	CH_3OH yield (%)
15	11.6	54.8	6.36
30	11.6	55.2	6.40
60	**11.8**	**58.7**	**6.93**
80	12.3	52.8	6.49
100	12.7	46.8	5.94

7. Reaction temperature at different residence time

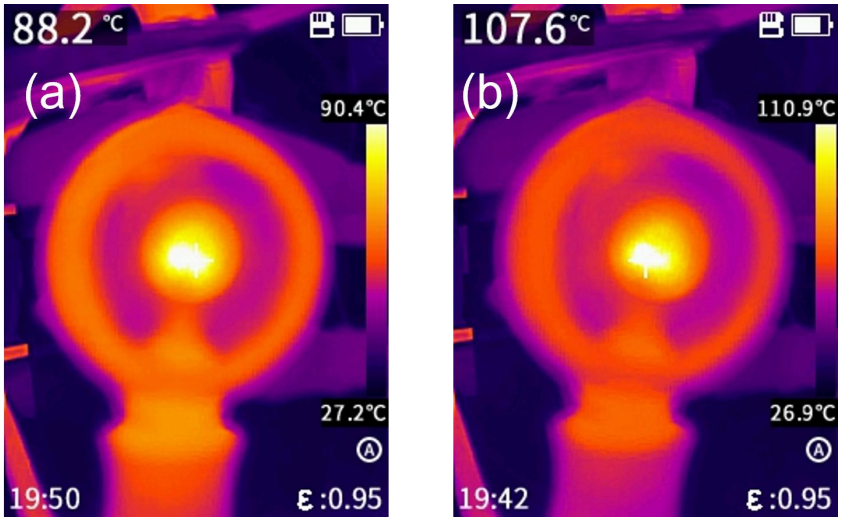

Figure S6. Reaction temperature at different residence time. (a) 4.7 s residence time; (b) 7 s residence time.

8. Plasma catalysis, thermal catalysis and electrocatalysis for CO_2 to CH_3OH

Table S2. Summary of plasma catalysis, thermal catalysis and electrocatalysis for CO_2 to CH_3OH.

Plasma catalysis in this paper

Catalyst	Conditions	CO_2 conversion (%)	CH_3OH selectivity (%)	Energy consumption (kJ/mmol)
Fe_2O_3/Al_2O_3	60 °C, 0.1 MPa	11.7	57.9	19.8
CuO/Al_2O_3	60 °C, 0.1 MPa	7.9	37.8	44.9
NiO/Al_2O_3	60 °C, 0.1 MPa	7.2	32.4	57.5
MoO_3/Al_2O_3	60 °C, 0.1 MPa	7.5	31.9	56.1
In_2O_3/Al_2O_3	60 °C, 0.1 MPa	6.8	33.3	59.2
CoO/Al_2O_3	60 °C, 0.1 MPa	7.4	28.1	64.5

Thermal catalysis

Catalyst	Conditions	CO_2 conversion (%)	CH_3OH selectivity (%)	STY (g_{MeOH} kg_{cat}^{-1} h^{-1})
$Cu/ZnO/Al_2O_3$ [1]	260 °C, 36 MPa	22.7	77.3	7729
$Cu/Zn/ZrO_2$ [2]	260 °C, 36 MPa	12	71.1	N/A
$CuNi_2/CeO_2$-NT [3]	260 °C, 3 MPa	17.8	78.8	579
$Cu_1La_{0.2}$/SBA-15 [4]	240 °C, 3 MPa	5.7	81.2	192
CuZnCe/TNTs [5]	260 °C, 3 MPa	23.3	59.8	298
CnZnZr/SBA-15 [6]	250 °C, 3 MPa	19.2	30.6	376
CnZnAl@HT(40%) [7]	250 °C, 3 MPa	6.2	74.7	42
LDH30Ga [8]	270 °C, 4.5 MPa	19	48	590
CuZnZr-LDH [9]	250 °C, 3 MPa	4.9	78.3	37
CuZnAl-400 [10]	240 °C, 4 MPa	59.5	73.4	128
$Cu/ZnO/ZrO_2/Ga_2O_3$ [11]	250 °C, 8 MPa	N/A	70	382
$Cu/Zn/Ga/SiO_2$ [12]	270 °C, 2 MPa	5.6	99.5	349
$Pd/ZnO–Al_2O_3$ [13]	180 °C, 3 MPa	2.9	79.4	N/A
Pd/Zn/CNTs [14]	250 °C, 3 MPa	6.3	99.6	1187
Pd/Zn [15]	220 °C, 2 MPa	14.1	97.2	166
0.5Ca5Pd5ZnZr [16]	230 °C, 3 MPa	7.2	100	64
Ag@Pd-ZnO [17]	270 °C, 4.5 MPa	18	46	280
$CdZrO_x$ [18]	300 °C, 2 MPa	5.4	80	N/A
$CuIn/SiO_2$ [19]	280 °C, 3 MPa	7.7	81.8	135
3La10In/ZrO2 [20]	300 °C, 4 MPa	7.7	66	420
Ni_5Ga_3/SiO_2-CP [21]	200 °C, 0.1 MPa	1.8	96.1	81
$Ni_5Ga_3/SiO_2/Al_2O_3/Al$ [22]	210 °C, 0.1 MPa	2.3	86.7	20

Au/ZnO [23]	240 °C, 0.5 MPa	0.3	82	N/A
In_2O_3/ZrO_2 [24]	300 °C, 5 MPa	5.2	99.8	321
Table S2 (continued)				
MoS_2 [25]	180 °C, 5 MPa	12.5	94.3	N/A
Al/Pd/ZnO [26]	250 °C, 3 MPa	14.2	7.3	628
NiO−In_2O_3 [27]	250 °C, 3 MPa	2.8	53	256
Cu/C_3N_4 [28]	150 °C, 3.2 MPa	N/A	95.5	134
Cu@UiO-66 [29]	260 °C, 4.5 MPa	13.1	78.8	796
Au/In_2O_3 [30]	275 °C, 5 MPa	7.7	78	470

Electrocatalysis

Catalyst/electrocatalysts	Electrolyte	Durability test	Electrode potential (V)	Faradaic efficiency (%)
$Cu_{1.63}Se(1/3)$ [31]	$PF_6/CH_3CN/H_2O$	—	-2.1 V vs. Ag/Ag^+	77.6
FeP NA/TM [32]	0.5 M $KHCO_3$	36 h	-0.2 V vs. RHE	80.2
Pt_xZn/C [33]	0.1 M $NaHCO_3$	16 h	-0.9 V vs. RHE	81.4
V-doped In_2O_3 [34]	0.1 M $KHCO_3$	—	-0.83V vs. RHE	15.8
RuO_2/TiO_2 [35]	0.5 M $NaHCO_3$	—	-0.8 V vs. SCE	60.5
Pd-Cu bimetallic aerogel [36]	BF_4 and H_2O	24 h	-2.1 V vs. Ag/Ag+	80
$Cu_2O_{(OL-MH)}$/Ppy [37]	0.5 M $KHCO_3$	15 h	-0.85 V vs. RHE	94.2
2-pyridinethiol@Pt-Au NPs [38]	0.1 M KNO_3	20 h	-0.2 V vs. Ag/AgCl	39
PD-Zn/Ag [39]	0.1 M $KHCO_3$	—	-1.4 V vs. RHE	10.5
$Cu_{63.9}Au_{36.1}$/NCF [40]	0.5 M $KHCO_3$	—	-1.1 V vs. SCE	15.9
CoPc-NH_2/CNT [41]	0.1 M $KHCO_3$	12 h	-1.0 V vs. RHE	32
BP NPs [42]	0.1 M $KHCO_3$	18 h	-0.5 V vs. RHE	92
$Cu_{0.8ML}$/THH Pd NCs [43]	0.1 M $NaHCO_3$	—	-0.46 V vs. RHE	19.5
CuSAs/TCNFs [44]	0.1 M $KHCO_3$	50 h	-0.9 V vs. RHE	44

9. Reaction performance with different packing

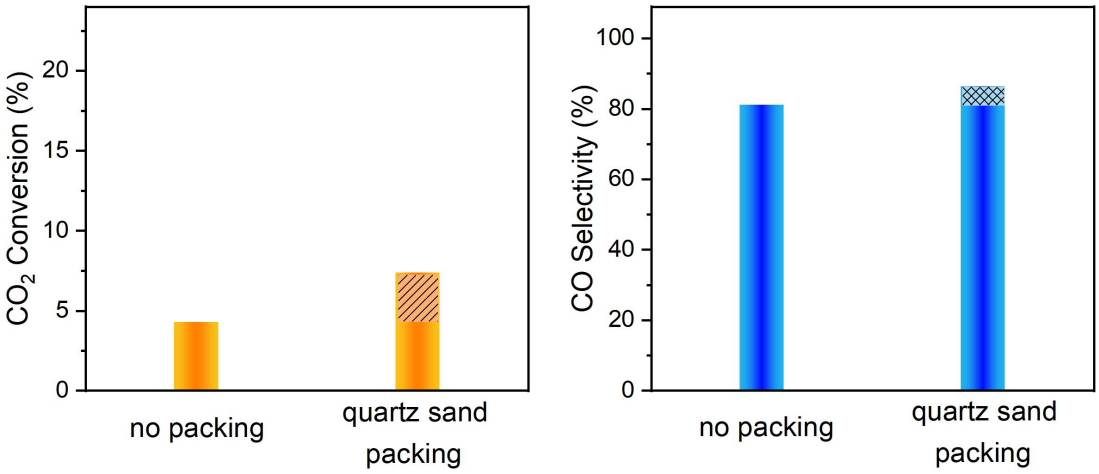

Figure S7. CO_2 conversion and CO selectivity with no packing and quartz sand packing. (discharge power 18 W, discharge frequency 9 kHz, $CO_2/H_2 = 1/3$, residence time 3.1 s, 60 °C circulating water, 1 atm pressure)

10. The average particle size and dispersion

Table S3. The average particle size and dispersion of Fe_2O_3 on γ-Al_2O_3 with various loadings.

Fe loading	2θ (degree)	β (rad)	τ (nm)	Average particle size(nm)	Dispersion percentage (%)
5 wt.%	35.7	0.59	13.99	15.02	6.39
	54.1	0.50	17.64		
	64.1	0.69	13.43		
10 wt.%	35.7	0.51	16.18	18.95	5.06
	54.1	0.43	20.51		
	64.1	0.46	20.15		
20 wt.%	24.3	0.32	25.11	22.31	4.30
	33.3	0.42	19.52		
	35.7	0.32	25.79		
	40.1	0.32	26.13		
	49.7	0.46	18.82		
	54.1	0.44	20.05		
	62.7	0.42	21.90		
	64.1	0.44	21.07		
	72.3	0.43	22.63		
	75.7	0.45	22.11		
25 wt.%	24.3	0.27	29.76	27.41	3.5
	33.3	0.30	27.33		
	35.7	0.26	31.74		
	40.1	0.28	29.87		
	49.7	0.32	27.05		
	54.1	0.33	26.73		
	62.7	0.38	24.21		
	64.1	0.40	23.17		
	72.3	0.39	24.95		
	75.7	0.34	29.26		

11. EDX mapping results

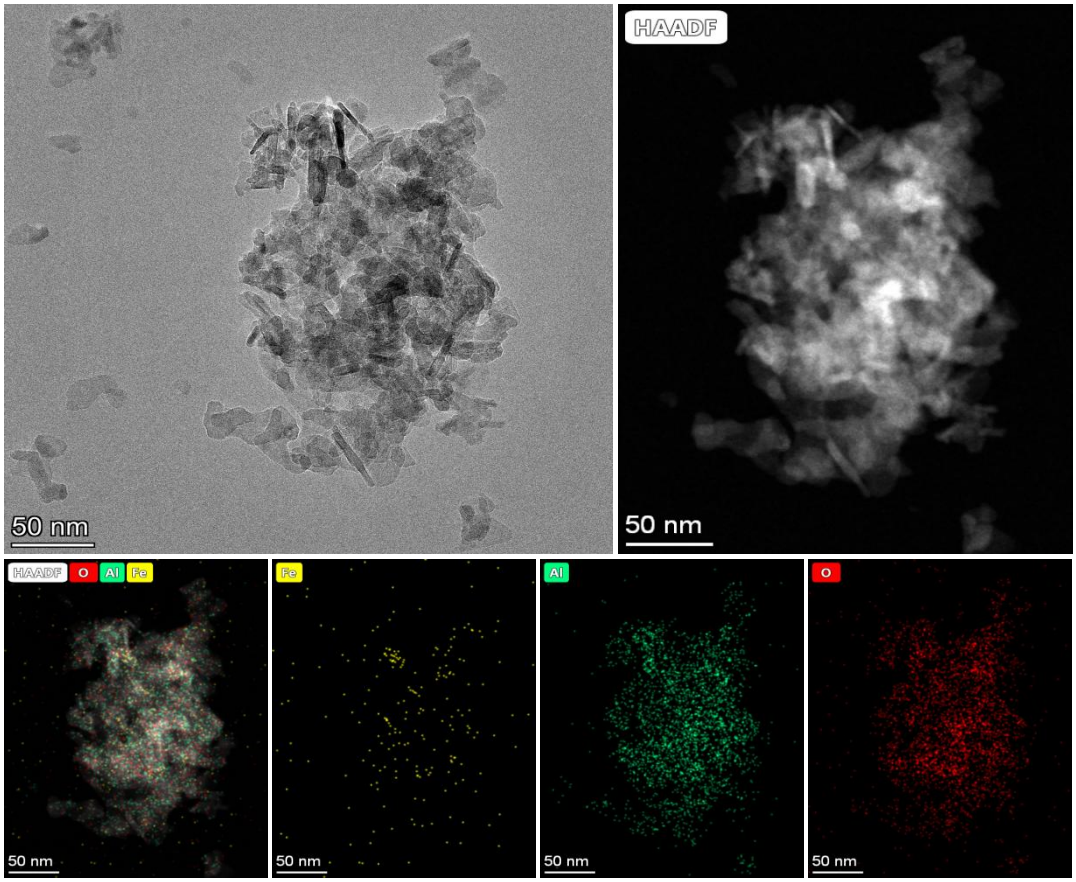

Figure S8. EDX mapping results of 5 wt.% $Fe_2O_3/\gamma\text{-}Al_2O_3$ catalysts.

12. N_2 physisorption data for the spent catalysts

Table S4. N_2 physisorption data for the spent catalysts.

Catalyst	S_{BET}[a] (m^2 g^{-1})	V_p (cm^3 g^{-1})	D[c] (nm)
γ-Al_2O_3	126.8	0.38	11.3
1 wt.% Fe_2O_3/γ-Al_2O_3	121.4	0.37	11.6
3 wt.% Fe_2O_3/γ-Al_2O_3	119.9	0.36	11.2
5 wt.% Fe_2O_3/γ-Al_2O_3	119.1	0.39	12.1
10 wt.% Fe_2O_3/γ-Al_2O_3	118.2	0.37	11.7
20 wt.% Fe_2O_3/γ-Al_2O_3	102.9	0.33	11.9
25 wt.% Fe_2O_3/γ-Al_2O_3	97.0	0.32	11.1
5 wt.% Fe_2O_3/$Al(OH)_3$	180.8	0.28	6.1
5 wt.% Fe_2O_3/SiO_2	149.3	0.56	14.6
5 wt.% Fe_2O_3/TiO_2	101.5	0.25	8.5
5 wt.% Fe_2O_3/CeO_2	49.9	0.10	8.1
5 wt.% Fe_2O_3/ZrO_2	32.0	0.15	23.6
5 wt.% Fe_2O_3/In_2O_3	15.5	0.08	20.7

[a] Specific surface area calculated with adsorption branch of nitrogen sorption isotherm using BET method.

[b] Total pore volume at $P/P_0 = 0.99$. [c] BJH Adsorption average pore diameter.

13. XPS results of CuO/γ-Al_2O_3 catalysts

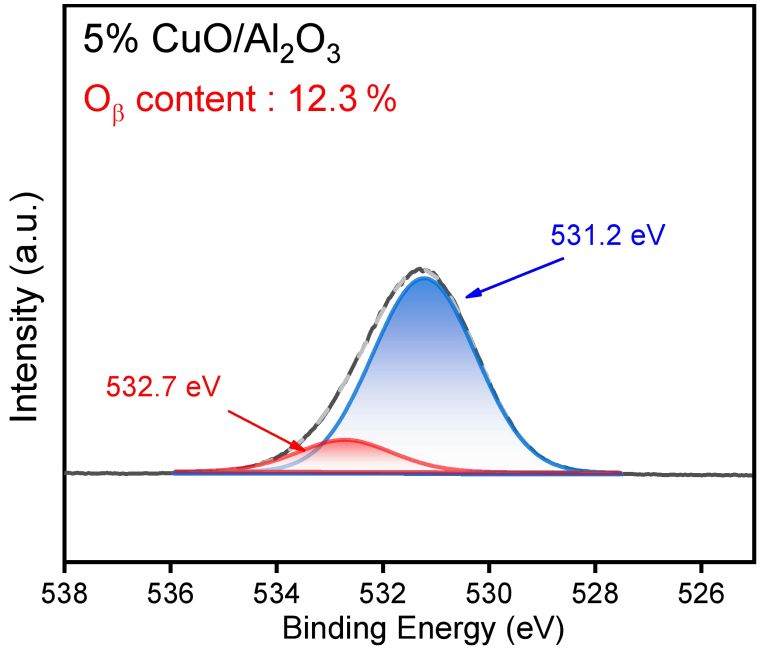

Figure S9. Cu 2p XPS spectra of CuO/γ-Al_2O_3 catalysts

14. XRD results of spent catalysts

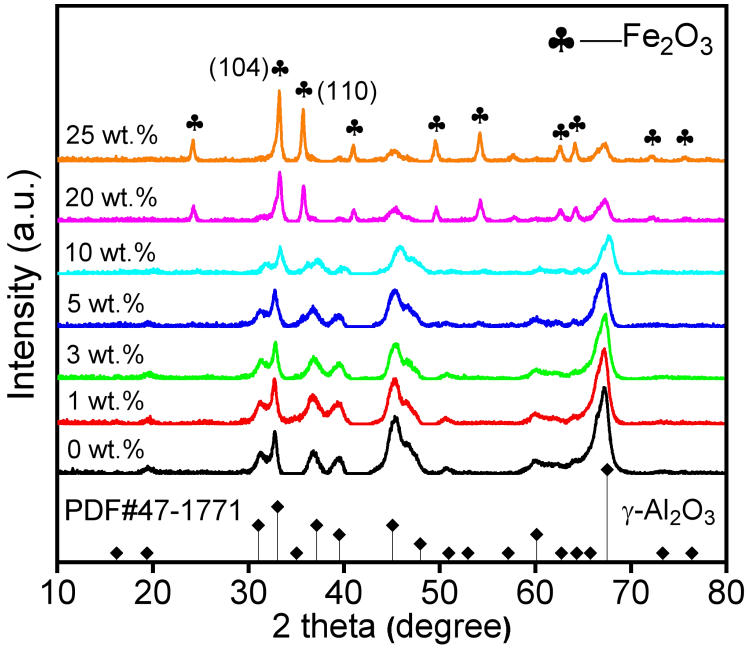

Figure S10. XRD patterns of the spent $Fe_2O_3/\gamma\text{-}Al_2O_3$ catalysts with various loadings.

15. Mössbauer parameters of fresh and spent 5 wt.% $Fe_2O_3/\gamma\text{-}Al_2O_3$ catalysts

Table S5. Mössbauer parameters of fresh and spent 5 wt.% $Fe_2O_3/\gamma\text{-}Al_2O_3$ catalysts.

	Iron Species	IS	QS	Line width	Magnetic filed	Spectra Contribution (%)
fresh catalyst	Fe_2O_3 (spm_1)	0.33	0.51	0.40	—	16.38
	Fe_2O_3 (spm_2)	0.26	1.07	0.80	—	37.95
	Fe_2O_3	0.34	-0.23	0.45	50.3	45.67
spent catalyst	Fe_2O_3 (spm_1)	0.35	0.53	0.4	—	18.18
	Fe_2O_3 (spm_2)	0.30	1.13	0.85	—	37.99
	Fe_2O_3	0.37	-0.21	0.45	50.3	43.83

16. TPR results of $Fe_2O_3/\gamma\text{-}Al_2O_3$ catalysts

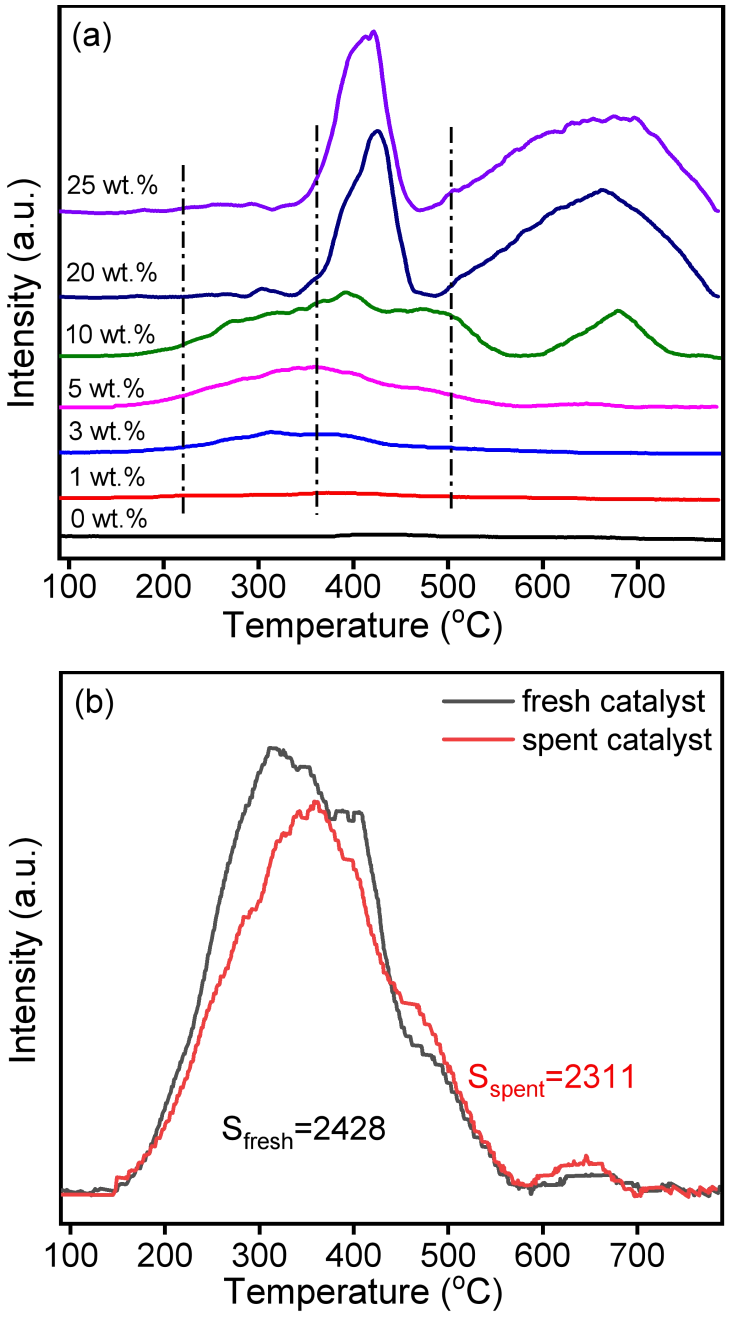

Figure S11. (a) H_2-TPR results of spent $Fe_2O_3/\gamma\text{-}Al_2O_3$ catalysts with various loadings; (b) Compare of H_2-TPR profiles of fresh and spent $Fe_2O_3/\gamma\text{-}Al_2O_3$ catalyst with 5 wt.% loading.

17. XPS results of spent catalysts

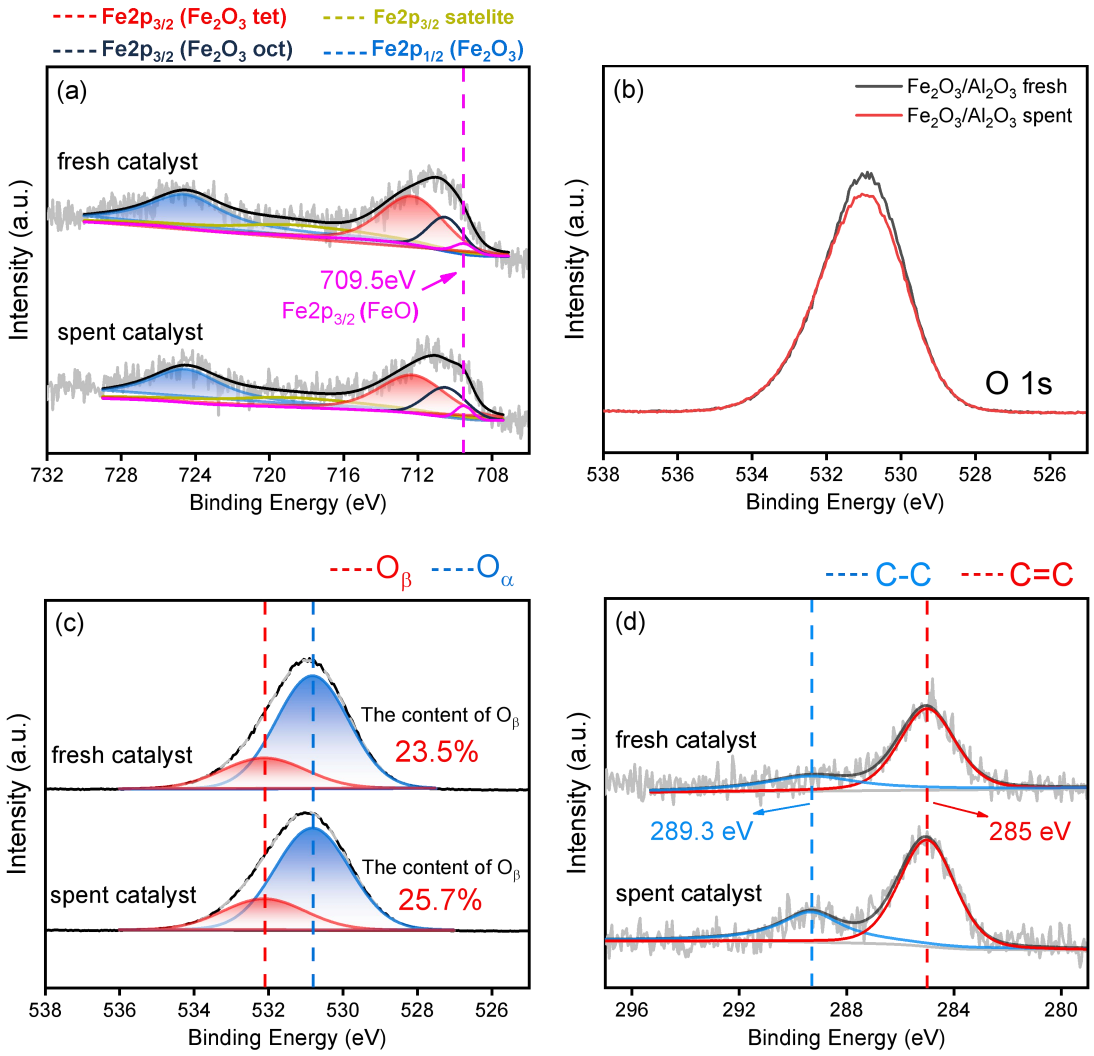

Figure S12. XPS results of spent $Fe_2O_3/\gamma\text{-}Al_2O_3$ catalysts with 5 wt.% loading: (a) Fe 2p regions; (b, c) O 1s regions; (d) C 1s regions.

18. HRTEM results of 5 wt.% $Fe_2O_3/\gamma\text{-}Al_2O_3$ spent catalyst

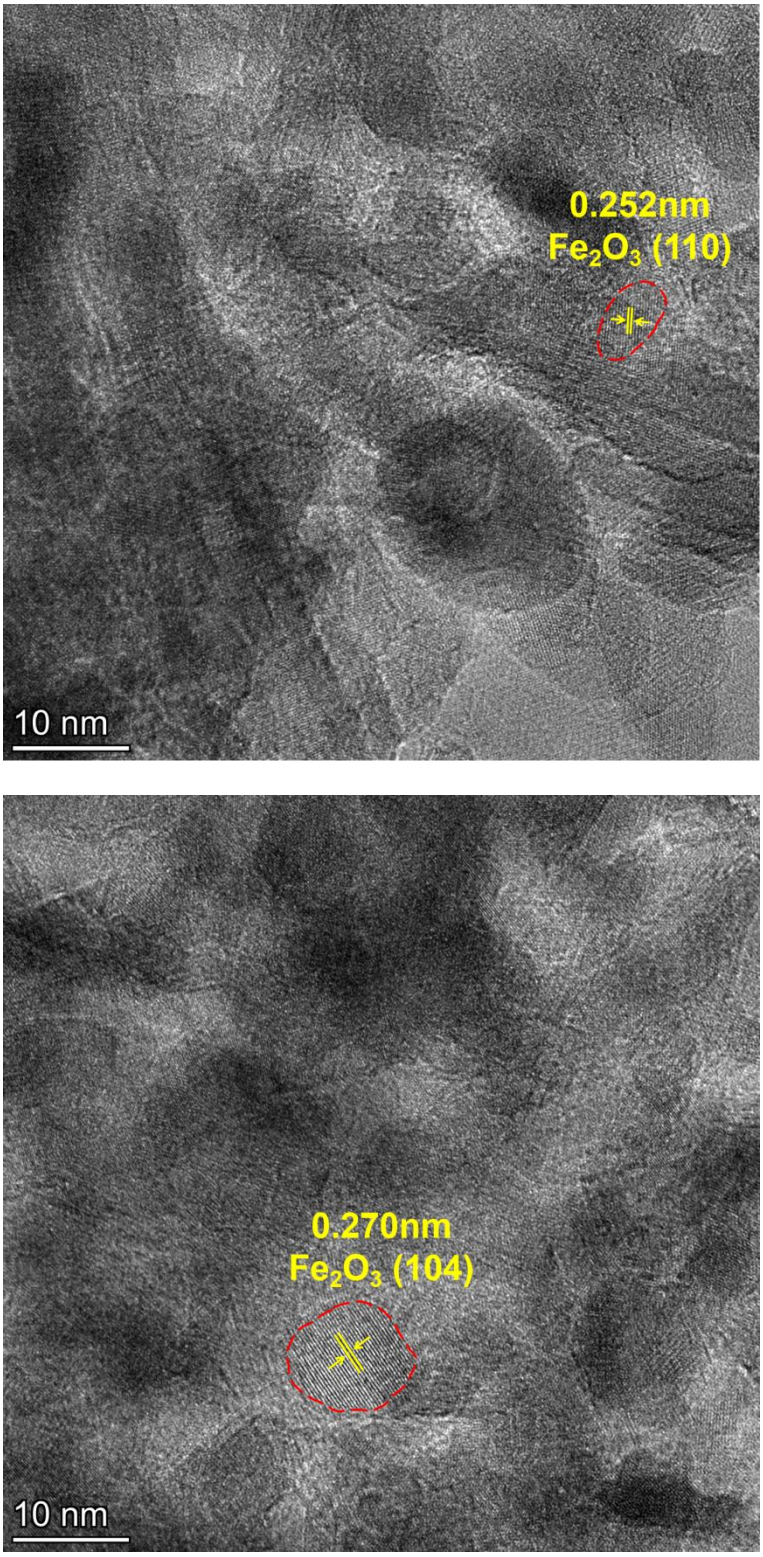

Figure S13. HRTEM results of 5 wt.% $Fe_2O_3/\gamma\text{-}Al_2O_3$ spent catalysts.

19. The reaction performance and H_2-TPR profiles of reduced catalyst

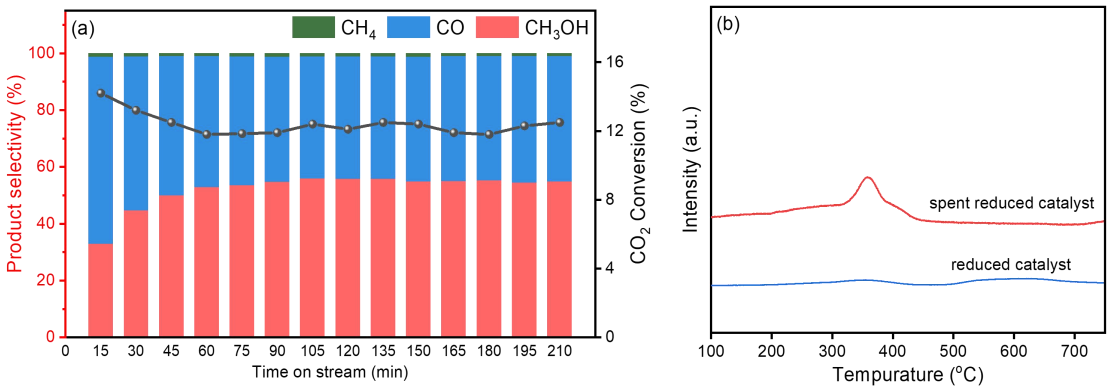

Figure S14. (a) The reaction performance of reduced catalyst; (b) H_2-TPR profiles of reduced catalyst and spent reduced catalyst.

20. UV-Vis spectrum of γ-Al_2O_3 and Fe_2O_3/γ-Al_2O_3

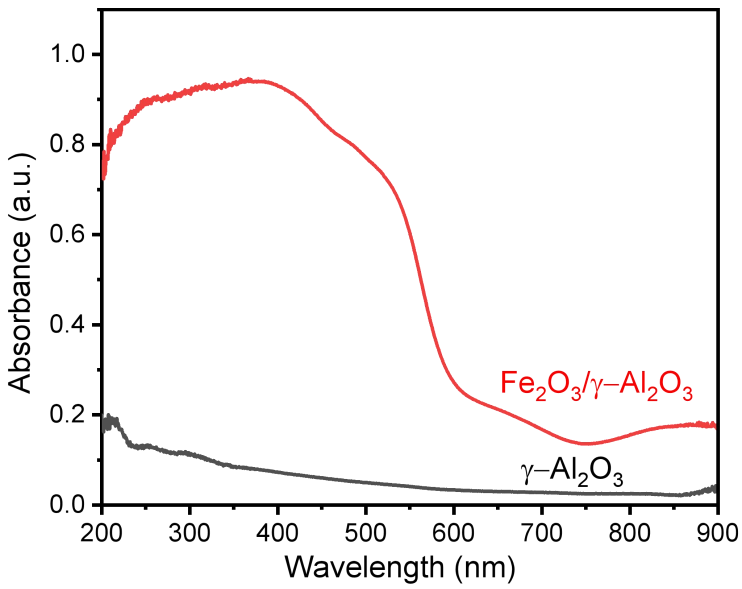

Figure S15. UV-Vis spectrum of γ-Al_2O_3 and Fe_2O_3/γ-Al_2O_3.

21. In situ DRIFTS reaction cell

In situ DRIFTS measurements were carried out using a FTIR spectrometer (Nicolet iS10, Thermo Scientific), equipped with a liquid N_2 cooled mercury-cadmium-telluride (MCT) detector. The catalyst (120 mg) was packed into the reaction cell (**Figure S16**) and pretreated in a CO_2/H_2 mixture (25 vol.% CO_2, 75 vol.% H_2) for 0.5 h before collecting the background. The plasma power was driven at 9.5 kHz with applied discharge voltage of 24 kV. The results were analyzed by the OMNIC software.

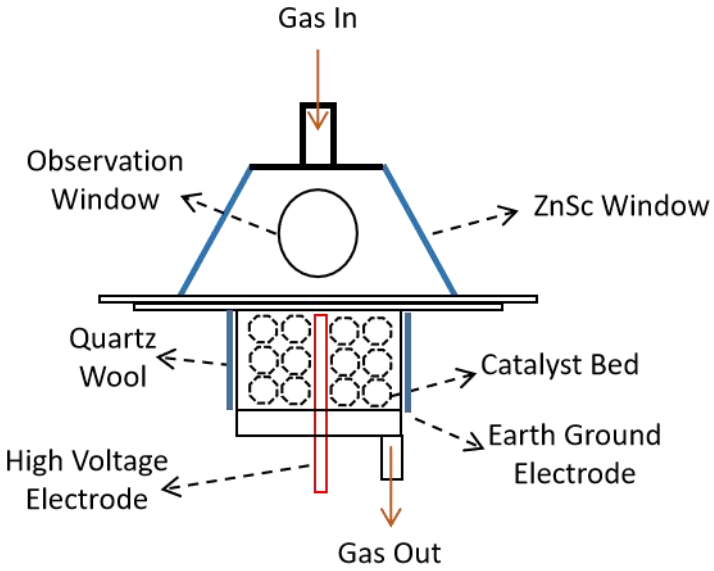

Figure S16. Schematic of in situ plasma reaction cell for a DRIFTS study.

22. In situ DRIFTS spectra of the linearly adsorbed CO_{ad}

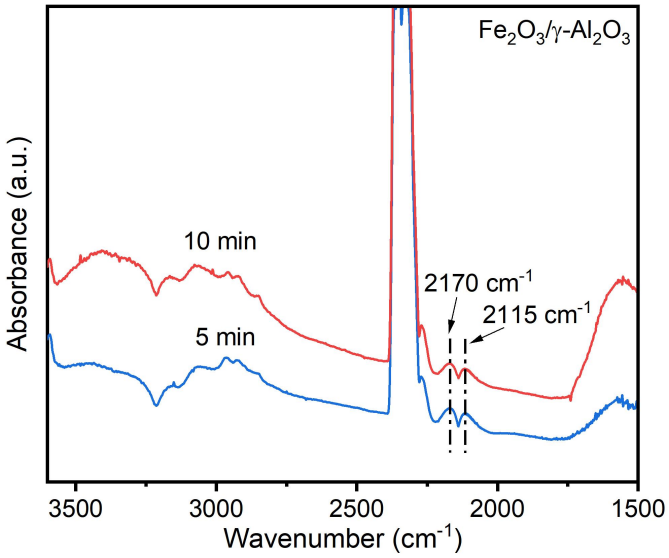

Figure S17. In situ DRIFTS spectra of surface species on the $Fe_2O_3/\gamma\text{-}Al_2O_3$ catalyst at the discharge power of 30.4 W. (discharge voltage 44 kV, discharge frequency 9.5 kHz, CO_2/H_2 = 1/3, flow rate =40 mL/min)

23. Possible E-R reactions in plasma-catalytic CO_2 hydrogenation to CH_3OH

Table S6. Possible E-R reactions in plasma-catalytic CO_2 hydrogenation to CH_3OH.

No	Reaction
1	H(g) + CO_2* – HCOO*
2	H(g) + CO_2* – COOH*
3	H(g) + CO* – HCO*
4	CO(g) + H* – HCO*
5	H(g) + HCOO* – HCOOH*
6	H(g) + H_3CO* – H_3COH*
7	H(g) + H_2COH* – H_3COH*

(g) denotes species from gas phase

24. References

[1] Bansode A, Urakawa A. Towards full one-pass conversion of carbon dioxide to methanol and methanol-derived products. *J. Catal*. 2014;309:66-70.

[2] Guo XM, Mao DS, Lu GZ, Wang S, Wu GS. Glycine-nitrate combustion synthesis of CuO-ZnO-ZrO_2 catalysts for methanol synthesis from CO_2 hydrogenation. *J. Catal*. 2010;271(2):178-185.

[3] Tan QQ, Shi ZS, Wu DF. CO_2 Hydrogenation to Methanol over a Highly Active Cu-Ni/CeO_2-Nanotube Catalyst. *Ind. Eng. Chem. Res*. 2018;57(31):10148-10158.

[4] Chen K, Fang HH, Wu S, et al. CO_2 hydrogenation to methanol over Cu catalysts supported on La-modified SBA-15: The crucial role of Cu-LaO_x interfaces. *Appl. Catal. B: Environ.* 2019;251:119-129.

[5] Shi ZS, Tan QQ, Wu DF. Enhanced CO_2 hydrogenation to methanol over TiO_2 nanotubes-supported CuO-ZnO-CeO_2 catalyst. *Appl. Catal. A Gen.* 2019;581:58-66.

[6] Mureddu M, Ferrara F, Pettinau A. Highly efficient CuO/ZnO/ZrO_2@SBA-15 nanocatalysts for methanol synthesis from the catalytic hydrogenation of CO_2. *Appl. Catal. B: Environ.* 2019;258:117941.

[7] Fang X, Men YH, Wu F, et al. Promoting CO_2 hydrogenation to methanol by incorporating adsorbents into catalysts: Effects of hydrotalcite. *Chem. Eng. J*. 2019;378:122052.

[8] Li MMJ, Chen CP, Ayvalı T, et al. CO_2 Hydrogenation to Methanol over Catalysts Derived from Single Cationic Layer CuZnGa LDH Precursors. *ACS Catal.* 2018;8(5):4390-4401.

[9] Fang X, Men YH, Wu F, et al. Improved methanol yield and selectivity from CO_2 hydrogenation using a novel Cu-ZnO-ZrO_2 catalyst supported on Mg-Al layered double hydroxide (LDH). *J. CO_2*

Util. 2019;29:57-64.

[10] Wu WY, Xie K, Sun DL, Li XH, Fang F. $CuO/ZnO/Al_2O_3$ Catalyst Prepared by Mechanical-Force-Driven Solid-State Ion Exchange and Its Excellent Catalytic Activity under Internal Cooling Condition. *Ind. Eng. Chem. Res*. 2017;56(29):8216-8223.

[11] Słoczyński J, Grabowski R, Olszewski P, et al. Effect of metal oxide additives on the activity and stability of $Cu/ZnO/ZrO_2$ catalysts in the synthesis of methanol from CO_2 and H_2. *Appl. Catal. A Gen.* 2006;310:127-137.

[12] Toyir J, de la Piscina PR, Fierro JLG, Homs N. Highly effective conversion of CO_2 to methanol over supported and promoted copper-based catalysts: influence of support and promoter. *Appl. Catal. B: Environ.* 2001;29(3):207-215.

[13] Xu JH, Su X, Liu XY, et al. Methanol synthesis from CO_2 and H_2 over $Pd/ZnO/Al_2O_3$: Catalyst structure dependence of methanol selectivity. *Appl. Catal. A Gen.* 2016;514:51-59.

[14] Liang XL, Dong X, Lin GD, Zhang HB. Carbon nanotube-supported Pd-ZnO catalyst for hydrogenation of CO_2 to methanol. *Appl. Catal. B: Environ.* 2009;88(3-4):315-322.

[15] Ojelade OA, Zaman SF, Daous MA, et al. Optimizing Pd:Zn molar ratio in $PdZn/CeO_2$ for CO_2 hydrogenation to methanol. *Appl. Catal. A Gen.* 2019;584:117185.

[16] Malik AS, Zaman SF, Al-Zahrani AA, Daous MA, Driss H, Petrov LA. Selective hydrogenation of CO_2 to CH_3OH and in-depth DRIFT analysis for $PdZn/ZrO_2$ and $CaPdZn/ZrO_2$ catalysts. *Catal. Today.* 2020;357:573-582.

[17] Li XL, Zeng ZY, Hu B, Qian LH, Hong XL. Surface-Atom Dependence of ZnO-Supported Ag@Pd Core@Shell Nanocatalysts in CO_2 Hydrogenation to CH_3OH. *ChemCatChem*. 2017;9(6):924-928.

[18] Wang JJ, Tang CZ, Li GN, et al. High-Performance M_aZrO_x (M_a = Cd, Ga) Solid-Solution Catalysts for CO_2 Hydrogenation to Methanol. *ACS Catal*. 2019;9(11):10253-10259.

[19] Shi ZS, Tan QQ, Wu DF. A novel Core-Shell structured CuIn@SiO_2 catalyst for CO_2 hydrogenation to methanol. *AIChE J*. 2019;65(3):1047-1058.

[20] Chou CY, Lobo RF. Direct conversion of CO_2 into methanol over promoted indium oxide-based catalysts. *Appl. Catal. A Gen*. 2019;583:117144.

[21] Ahmad K, Upadhyayula S. Conversion of the greenhouse gas CO_2 to methanol over supported intermetallic Ga-Ni catalysts at atmospheric pressure: thermodynamic modeling and experimental study. *Sustain. Energy Fuels*. 2019;3(9):2509-2520.

[22] Chen PJ, Zhao GF, Liu Y, Lu Y. Monolithic $Ni_5Ga_3/SiO_2/Al_2O_3$/Al-fiber catalyst for CO_2 hydrogenation to methanol at ambient pressure. *Appl. Catal. A Gen.* 2018;562:234-240.

[23] Hartadi Y, Widmann D, Behm RJ. CO_2 Hydrogenation to Methanol on Supported Au Catalysts under Moderate Reaction Conditions: Support and Particle Size Effects. *ChemSusChem*. 2015;8(3):456-465.

[24] Martin O, Martín AJ, Mondelli C, et al. Indium Oxide as a Superior Catalyst for Methanol Synthesis by CO_2 Hydrogenation. *Angew. Chem. Int. Ed.* 2016;55(21):6261-6265.

[25] Hu JT, Yu L, Deng J, et al. Sulfur vacancy-rich MoS_2 as a catalyst for the hydrogenation of CO_2 to methanol. *Nat Catal*. 2021;4(3):242-250.

[26] Song JM, Liu SH, Yang CS, et al. The role of Al doping in Pd/ZnO catalyst for CO_2 hydrogenation to methanol. *Appl. Catal. B: Environ*. 2020;263:118367.

[27] Zhu JD, Cannizzaro F, Liu L, et al. Ni-In Synergy in CO_2 Hydrogenation to Methanol. *ACS Catal.* 2021;11(18):11371-11384.

[28] Yang T, Mao XN, Zhang Y, et al. Coordination tailoring of Cu single sites on C_3N_4 realizes selective CO_2 hydrogenation at low temperature. *Nat. Commun.* 2021;12(1):1-9.

[29] Liu TK, Hong XL, Liu GL. In Situ Generation of the Cu@3D-ZrO_x Framework Catalyst for Selective Methanol Synthesis from CO_2/H_2. *ACS Catal*. 2019;10(1):93-102.

[30] Rui N, Zhang F, Sun KH, et al. Hydrogenation of CO_2 to Methanol on a $Au^{\delta+}$-In_2O_{3-x} Catalyst. *ACS Catal.* 2020;10(19):11307-11317.

[31] Yang DX, Zhu QG, Chen CJ, et al. Selective electroreduction of carbon dioxide to methanol on copper selenide nanocatalysts. *Nat. Commun*. 2019;10(1):1-9.

[32] Ji L, Li L, Ji XQ, et al. Highly Selective Electrochemical Reduction of CO_2 to Alcohols on a FeP Nanoarray. *Angew. Chem. Int. Ed.* 2020;132(2):768-772.

[33] Payra S, Shenoy S, Chakraborty C, Tarafder K, Roy S. Structure-Sensitive Electrocatalytic Reduction of CO_2 to Methanol over Carbon-Supported Intermetallic PtZn Nano-Alloys. *ACS Appl. Mater. Inter*. 2020;12(17):19402-19414.

[34] Kim MG, Jeong J, Choi Y, et al. Synthesis of V-doped In_2O_3 Nanocrystals via Digestive-Ripening Process and Their Electrocatalytic Properties in CO_2 Reduction Reaction. *ACS Appl. Mater. Inter*. 2020;12(10):11890-11897.

[35] Qu JP, Zhang XG, Wang YG, Xie CX. Electrochemical reduction of CO_2 on RuO_2/TiO_2 nanotubes composite modified Pt electrode. *Electrochim. Acta*. 2005;50(16-17):3576-3580.

[36] Lu L, Sun XF, Ma J, et al. Highly Efficient Electroreduction of CO_2 to Methanol on Palladium-Copper Bimetallic Aerogels. *Angew. Chem. Int. Ed.* 2018;130(43):14345-14349.

[37] Periasamy AP, Ravindranath R, Kumar SMS, Wu WP, Jian TR, Chang HT. Facet- and structure-dependent catalytic activity of cuprous oxide/polypyrrole particles towards the efficient

reduction of carbon dioxide to methanol. *Nanoscale*. 2018;10(25):11869-11880.

[38] Ensafi AA, Alinajafi HA, Jafari-Asl M, Rezaei B. Self-assembled monolayer of 2-pyridinethiol@Pt-Au nanoparticles, a new electrocatalyst for reducing of CO_2 to methanol. *J. Electroanal. Chem.* 2017;804:29-35.

[39] Low QH, Loo NWX, Calle-Vallejo F, Yeo BS. Enhanced Electroreduction of Carbon Dioxide to Methanol Using Zinc Dendrites Pulse-Deposited on Silver Foam. *Angew. Chem. Int. Ed*. 2019;58(8):2256-2260.

[40] Jia FL, Yu XX, Zhang LZ. Enhanced selectivity for the electrochemical reduction of CO_2 to alcohols in aqueous solution with nanostructured Cu-Au alloy as catalyst. *J. Power Sources*. 2014;252:85-89.

[41] Wu YS, Jiang Z, Lu X, Liang YY, Wang HL. Domino electroreduction of CO_2 to methanol on a molecular catalyst. *Nature*. 2019;575(7784):639-642.

[42] Mou SY, Wu TW, Xie JF, et al. Boron Phosphide Nanoparticles: A Nonmetal Catalyst for High-Selectivity Electrochemical Reduction of CO_2 to CH_3OH. *Adv. Mater*. 2019;31(36):1903499.

[43] Zhang FY, Sheng T, Tian N, et al. Cu overlayers on tetrahexahedral Pd nanocrystals with high-index facets for CO_2 electroreduction to alcohols. *Chem. Commun*. 2017;53(57):8085-8088.

[44] Yang HP, Wu Y, Li GD, et al. Scalable Production of Efficient Single-Atom Copper Decorated Carbon Membranes for CO_2 Electroreduction to Methanol. *J. Am. Chem. Soc.* 2019;141(32):12717-12723.